foundations

MDPI

Article

Knots in Polymer Molecules Under Poiseuille Flow

Maurice P. Schmitt [1] and Andrey Milchev [2,*]

[1] Institut für Physik, Johannes Gutenberg-Universität, 55128 Mainz, Germany
[2] Institute of Physical Chemistry, Bulgarian Academy of Sciences, 1113 Sofia, Bulgaria
* Correspondence: milchev@ipc.bas.bg

Abstract

Knots are ubiquitous in polymers and biological macromolecules such as DNA and proteins, yet their behavior and functionality are still not sufficiently explored. Here we investigate the impact of Poiseuille flow on simple knots in flexible polymers placed in a quasi-rectangular micro-channel by systematically varying the flow strength for different chain lengths. Hydrodynamic interactions are accounted for by means of Multi-Particle Collision Dynamics (MPCD). We find that initially loosely localized knots in polymer coils typically *tighten* under shear to several segments beyond a certain body force threshold. At higher shear rates, intermittent transition from chain stretching to tumbling is observed which correlates with strong fluctuations in the knot size. Somewhat unexpectedly, our results indicate that the influence of channel width on tightening steadily increases with growing width even at *equal* mean shear rate $\bar{\dot{\gamma}}$.

Keywords: knot dynamics; shear flow; polymers; Alexander polynomial; molecular dynamics

1. Introduction

The biological role of knots in living matter, in particular their impact on enzymes and the kinetic stability of proteins [1] is of significant importance. Yet despite intensive studies in recent years, it is still not well understood. Knots are ubiquitous in polymers [2] and biological molecules [3], such as DNA [4–8] and proteins [9–16]. Knots become exponentially more common as the polymer length [17–20] or compactness increases [21,22]. Though formally defined in closed rings [23], open knots can be identified using suitable closures [24,25]. Knots tie and untie spontaneously via the polymer ends. In a polymer melt, for example, this occurs by the slithering motion of the polymer chains [26–28]. Their formation is often promoted by chain stiffness [29] or confinement. External forces influence knots differently depending on how the force is applied. Knots can either tighten [30] or untie [31] when pulling forces, for example, those applied in single-molecule experiments [32], are applied. However, the impact of common forces like shear (in its variety) on knots still poses a number of open questions, most notably, on whether knots generally rather tighten or untie subject to a particular type of flow.

Prior studies have shown that single *ring* polymers under simple (Couette) shear [33] exhibit a tumbling motion, which leads to a broad distribution of knot sizes, rather than fully tightened knots at all times. For linear chains an investigation on dynamics and topology of knots in steady shear flow [34] revealed repeated unknotting–knotting transitions in flexible chains. This is in contrast to Brownian dynamics simulations on the behavior of knotted chains in elongational flow [35], which have concluded earlier that knots untie. Other studies have driven knots by exposing knotted polymers to AC/DC fields [36]. In

check for updates

Academic Editor: T. M. Indra Mahlia

Received: 10 June 2025
Revised: 26 July 2025
Accepted: 29 July 2025
Published: 13 August 2025

Citation: Schmitt, M.P.; Milchev, A. Knots in Polymer Molecules Under Poiseuille Flow. *Foundations* **2025**, *5*, 28. https://doi.org/10.3390/foundations5030028

Copyright: © 2025 by the authors. Licensee MDPI, Basel, Switzerland. This article is an open access article distributed under the terms and conditions of the Creative Commons Attribution (CC BY) license (https://creativecommons.org/licenses/by/4.0/).

recent years, DNA knots stretched by elongational fields have been studied experimentally, where particular interests are the relaxation [37], dynamics [38], attraction [39], and untying [40] of the knots. Very recently, we demonstrated [41] that knots present in a linear polymer always *tighten* when placed in a Couette flow. In contrast to knots, the impact of shear on the conformational and dynamic evolution of polymer chains themselves has been the subject of intensive investigations for several decades now [42–47] and is currently much better understood.

While the influence of shear and elongational flows on knotted polymer chains has been studied previously, the specific case of Poiseuille flow presents a fundamentally distinct scenario that merits independent investigation. Unlike steady shear flow, which imposes a uniform velocity gradient, Poiseuille flow introduces spatial heterogeneity in the shear rate across the channel, leading to non-trivial polymer conformational dynamics. Prior studies have demonstrated that such flow fields induce local structural and orientational features that are not captured by linear shear flow [cf. Gompper et al. [48]]. Moreover, elongational flows—although also involving deformation—tend to untie rather than contract knots, highlighting the sensitive dependence of knot behavior on the flow details [35,37,40]. Given the absence of systematic studies on the impact of Poiseuille flow on intra-chain knots, and considering the relevance of such flow in microfluidic and biological environments, the present work addresses a critical gap in the literature and provides novel insights into the interplay between knot topology and non-uniform flow fields and gradients.

2. Model

We adopt a coarse-grained approach to describe the segments, modeling a polymer chain as a bead–spring system, where N effective spherical monomeric units are connected by appropriate effective potentials. Any two beads (i, j) in the system, separated by a distance $r = |\vec{r}_i - \vec{r}_j|$, interact through the purely repulsive Weeks–Chandler–Andersen (WCA) potential:

$$U^{WCA}(r) = \quad 4\epsilon\left[\left(\frac{\sigma}{r}\right)^{12} - \left(\frac{\sigma}{r}\right)^{6} + \frac{1}{4}\right], \quad \text{if} \quad r \le r_c = 2^{1/6}\sigma; \quad 0 \quad \text{if} \quad r > 2^{1/6}\sigma. \tag{1}$$

ϵ determines the interaction strength in units of thermal energy $k_B T$, while σ defines the characteristic interaction range. We use reduced units where $\epsilon = 1$ and $\sigma = 1$. Consecutive monomers along the polymer chain are connected via the finitely extensible nonlinear elastic (FENE) potential [49],

$$U^{\text{FENE}}(r) = \; -0.5kr_0^2 \ln\left[1 - \left(\frac{r}{r_0}\right)^2\right] \quad \text{if} \quad r < r_0; \quad \infty \quad \text{if} \quad r \ge r_0. \tag{2}$$

with standard parameter values $r_0 = 1.5\sigma$ and $k = 30\epsilon/\sigma^2$. Equations (1) and (2) establish a well-defined bond length of $\ell_b \approx 0.97\,\sigma$, with fluctuations limited to approximately $0.03\,\sigma$, independent of chain stiffness. In this work, we examine fully flexible polymer chains consisting of $N = 512$ or $N = 1024$ athermal segments, maintaining a constant temperature of $T = 1\,\epsilon/k_B$ across all simulations.

The polymer chains are confined to a slit environment, bounded by smooth repulsive walls that extend along the X-axis and are normal to the Z-axis. The simulation box dimensions are set to $L_x \times L_y \times L_z = 200 \times 80 \times 80$ for chains with $N = 512$ and $200 \times 160 \times 160$ for those with $N = 1024$. At equilibrium in the absence of shear, the polymer's mean radius of gyration, $\langle R_g^2 \rangle = N^{-2} \sum_{i=1, j>i}^{N} \langle (\vec{r}_i - \vec{r}_j)^2 \rangle$, is measured as $\langle R_{g0}(N = 512) \rangle = 18.85$ and $\langle R_{g0}(N = 1024) \rangle = 32.91$. To integrate the equations of motion, we employ the NVE en-

semble for the chain segments while temperature equilibration is incorporated in the MPCD method by an NVT ensemble , with a time step of $dt_{MD} = 0.0003\,\tau_{MD}$ for $N = 256, 512$, and $0.00025\,\tau_{MD}$ for $N = 1024$. Here, the fundamental molecular dynamics time unit is given by $\tau_{MD} = \sqrt{m\sigma^2/\epsilon}$.

In the Multi-Particle Collision Dynamics (MPCD) method, solvent particles are treated as ideal point particles with unit mass $m = 1$ and follow alternating streaming and collision steps [50,51]. During the streaming phase, solvent particles move ballistically over a time interval of $dt_{\mathrm{MPCD}} = 0.0025\tau_{MD}$. In the collision phase, particles are sorted into cubic cells of volume σ^3 (with a numeric density of $\rho = 5\sigma^{-3}$ per cell), where they undergo stochastic momentum exchanges while conserving both local and global momentum. Collisions occur at intervals of $10 \times dt_{MPCD}$.

We utilize the HOOMD-Blue $v2.9.4$ software package [52] on GPUs, incorporating an Andersen thermostat collision scheme [53] to regulate temperature and bounce-back collisions at the confining walls to ensure no-slip boundary conditions. Before each collision phase, cells are displaced randomly by a three-dimensional vector with components uniformly drawn from $[-\sigma/2, \sigma/2]$, and the velocities of MPCD particles are rotated by an angle of $\alpha = 130^\circ$ relative to the center-of-mass velocity, ensuring Galilean invariance [54].

In the Poiseuille flow setup, a uniform body force with magnitude f is exerted on the solvent in the X-direction, driving the fluid. When polymer concentration is low, the solvent behaves as a Newtonian fluid with viscosity η, generating the well-known characteristic parabolic velocity distribution:

$$v_x(z) = \frac{\rho f}{2\eta}\left(\frac{L_z^2}{4} - z^2\right). \tag{3}$$

The flow intensity is characterized by the mean shear rate $\bar{\dot{\gamma}} = fH/2\nu$ [48,55], representing the shear rate averaged across the channel. Here, $H = L_z/2$ denotes the channel half-width, while $\nu = \eta/\rho$ corresponds to the kinematic viscosity. Since the kinematic viscosity is constant, we characterize the mean shear rate by the value of $\bar{\dot{\gamma}} \cdot \nu$ later in this study.

To express our results in hydrodynamic terms, we define the Weissenberg number as $\mathrm{Wi} = \dot{\gamma}\tau_0$, where τ_0 represents the longest relaxation time of the polymer chain. This relaxation time is determined by examining the exponential decay of the autocorrelation function:

$$C(t) = \frac{\langle \vec{R}(t_0 + t)\vec{R}(t_0)\rangle}{\langle \vec{R}(t_0)\vec{R}(t_0)\rangle} = \exp(-t/\tau_0), \tag{4}$$

where $\vec{R}(t)$ is the polymer's end-to-end vector (shifted by its mean), and t_0 is a reference time. For a coil of length $N = 512$, we find $\tau_0 = 31{,}892\,\tau_{MD}$, while for $N = 1024$, $\tau_0 = 214{,}285.5\,\tau_{MD}$. Our model for a Poiseuille flow [56] yields a value of $\eta/\rho = 2.83\,k_BT\,\tau_{MD}$ for the kinematic viscosity, where η is the dynamics viscosity of the fluid. Thus, one obtains the Reynolds number $Re = v\rho L_z/\eta \approx 1.7$ for a velocity v at body force $f = 0.004$.

In the swollen coil state, the likelihood of encountering a knot in these chain lengths is generally around 1% or lower [22]. Knots in this regime tend to be weakly localized, occupying only a portion of the polymer and undergoing continuous fluctuations in both size and position along the contour.

Throughout simulations, we track the position and size of a pre-existing knot, which is initially introduced as a trefoil knot selected from equilibrium configurations. Knot analysis is conducted using the KymoKnot package [57], which identifies the knot type, location,

and size by computing the Alexander polynomial [23] with a minimally interfering closure. Knot size determination follows a bottom-up approach, progressively incorporating monomers until a knotted region consistent with the overall chain topology is identified. The minimally interfering closure either connects the chain termini directly or joins them through the shortest distance to the convex hull, depending on whether the direct distance between the ends is shorter than the summed minimal distances of the termini to the convex hull of the polymer. Alternative methods for detecting knots in open chains without prior closure have also been developed [58,59].

3. Results

3.1. Effect of Shear on Knot Size in a Poiseuille Flow

We show in Figure 1a the temporal changes in knot size $K_n(t)$ over a longer period of time in a channel at zero body force f demonstrating that in the absence of shear K_n undergoes moderate fluctuations of $\pm 21\%$ around its mean size (here $\langle K_n(t) \rangle = 116.35$). Although the knot position undergoes a certain diffusion along the chain contour, (e.g., the center of the trefoil knot K_n-mid diffuses over $\approx$60 beads from its initial position in the polymer chain over the course of the simulation in Figure 1a), its location is found to change little during the whole time interval, similar to the radius of gyration, $R_g(t)$, of the chain. When a constant body force f is applied to the fluid particles, the polymer chain starts moving in the resulting flow. Beyond a certain threshold value f^{cr}, the knot undergoes a process of tightening at a rate which is found to increase linearly with the growing force f, shown in Figure 1b. Apparently, the tightening rate $\dot{K}_n = dK_n(t)/dt$ (determined from the slope of a linear fit to $K_n(t)$ during the tightening process, more details in Supplementary Section S1) of the long chain, $N = 1024$, is significantly larger due to the stronger local shear acting on its building units. Figure 2 shows a series of snapshots of a knot, taken at different moments after the onset of flow, clearly demonstrating the gradual tightening of the knot down to only a few remaining beads. Note that in this study we employ only weak to moderate forces since rather strong body forces f may lead to knot removal by intersegmental passage. While this results in knot elimination similar to the action of type II topoisomerase in DNA [60], the underlying mechanisms are fundamentally different. The Supplementary Video provides a visualization of a possible stretched conformation, where the chain ends fall into regions in the vicinity of the walls where the flow is slower.

The variation of the knot size $K_n(t)$ in polymer chains with length $N = 512$ and $N = 1024$ with elapsed time is shown in Figure 3. While for $N = 512$ and $f = 5 \times 10^{-5}$ the knot size stays largely constant, Figure 3a, for $f \geq 10^{-4}$ one observes a steady decline of K_n, which becomes faster with growing f along with intermittent short-lived fluctuations. The same qualitative observation is made for $N = 1024$, although tightening occurs at lower body forces due to the larger shear on the larger chain. Note that occasional sudden changes (spikes) in the knot size are caused by the knot detection scheme, which can measure significantly different knot lengths between frames due to the closure scheme necessary for open chains (e.g., the minimally interfering closure of KymoKnot might use its bridging closure in one frame and the outer closure in the next; more details in Ref. [57]).

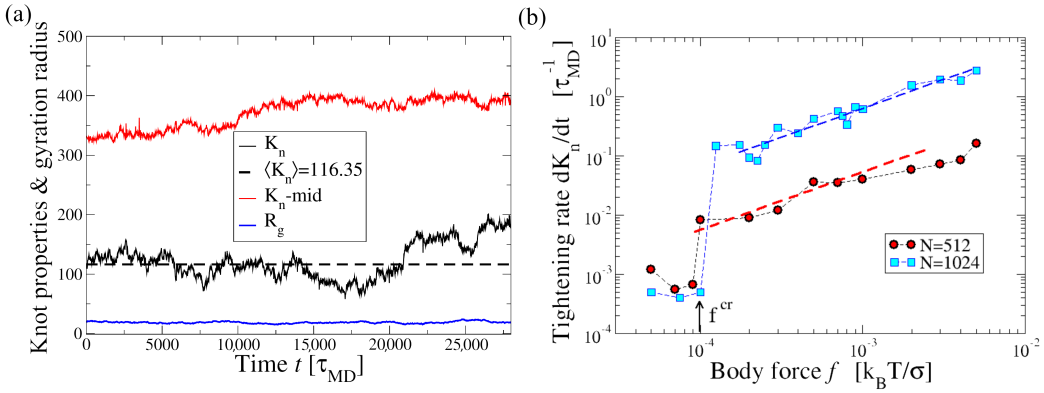


Figure 1. (**a**) Knot size, K_n, over time (black), and diffusive motion of the knot middle monomer along the chain (red) in units of monomer indices for a chain with $N = 512$ at zero shear flow $\dot{\gamma} = 0$. The change in R_g (in simulation length units σ) with time is indicated by a blue line while $\langle R_g \rangle \approx 18.85$. (**b**) The onset of shear tightening and increase in the shear tightening rate $\dot{K}_n$ with growing body force f for chain lengths $N = 512$, $N = 1024$. The critical (threshold) value is $f^{cr} \approx 10^{-4}$.

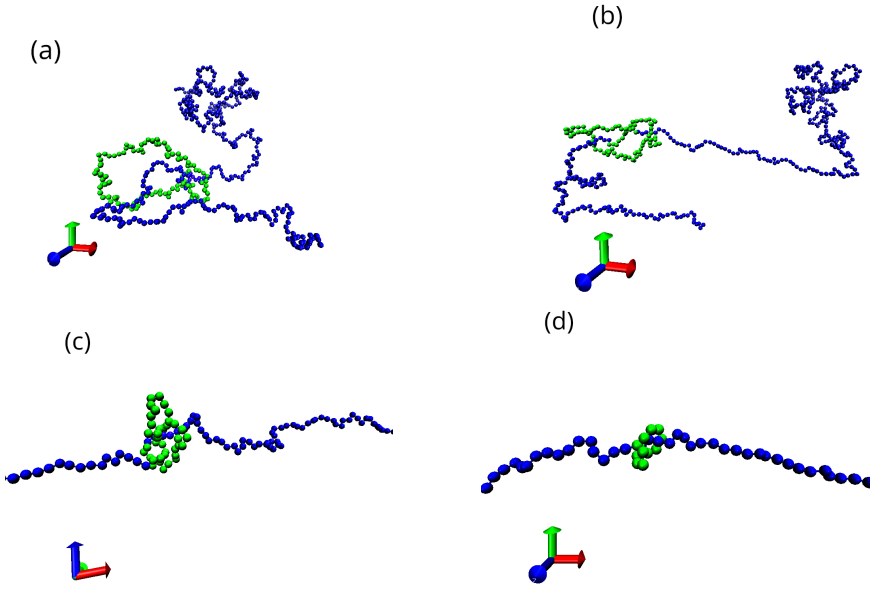


Figure 2. Tightening of a trefoil knot of size $K_n(t)$ in a chain with $N = 512$ segments with elapsed time (in units of τ_{MD}) after the onset of flow due to body force $f = 0.0005$. Thus, $K_n(300\tau_{MD}) = 113$ (**a**), $K_n(600\tau_{MD}) = 90$ (**b**), $K_n(1200\tau_{MD}) = 41$ (**c**) and $K_n(1800\tau_{MD}) = 10$ (**d**). The knotted section (as determined by the KymoKnot software package) is depicted in green. All plots are prepared with VMD [61].

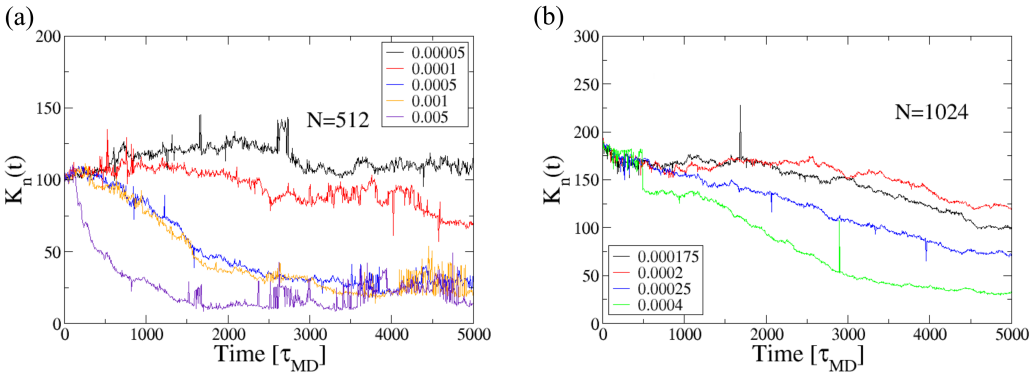


Figure 3. Average knot tightening over 9 simulation runs for each body force vs. time for several values of the body force f (given as a parameter) for (**a**) chain length $N = 512$, and (**b**) $N = 1024$.

3.2. Cross-Correlation Between Chain Tumbling and Knot Size

Generally, the type of flow strongly affects the conformational response of the polymer molecule. Similar to the case of simple shear [41,62], one observes large conformational fluctuations in pressure-driven flow with a Poiseuille profile, whereby the polymer chain stretches and recoils [48]. In addition to tumbling dynamics, however, the transverse migration of polymers toward the center line of the channel is observed [55].

Our observations reveal an immediate relation between the appearance of recoil conformations and the ensuing abrupt changes in knot size. As shown in Figure 4a, the size distributions of trefoil knots for two different forces f differ markedly, revealing considerably larger knots for the weaker body force $f = 0.00009$. Moreover, as suggested by the inset to Figure 4a, knots close to the minimum or maximum x-position relative to the chain (or 'outer' knots) are generally larger than those with central (or 'inner') relative x-positions if $f \gg f^{cr}$ (here, the relative x-position refers to the range of x-positions between the monomer with the smallest x-coordinate and the monomer with the largest x-position). This is due to the larger elongational forces acting on the center of the chain. The long tail of the overall trefoil length distribution at $f = 0.00165$ is thus shown to be predominantly caused by knots with outer relative x-positions, while the occurrences of very tight trefoil knots are predominantly caused by knots with inner relative x-position. This point is further illustrated by Figure 4b: When the knot positions (snapshots, bottom of the panel) are far from the relative termini $x_{\mathrm{rel}} = 0$ or $x_{\mathrm{rel}} = 100\,\%$ then the knot size is small (cf. inset in Figure 4a), and the knot position is constant, indicated by the fairly thin and constant kymograph bands (spanning from knot start to knot end positions) in the top of the panel in Figure 4b. Conversely, if the knots lie close to the relative end points of the chain, then the knot becomes larger and the knot center can move. Since the knot thus alternates between tightened and loose states as the polymer tumbles, the knot is "breathing" [63]. This correlation between tumbling and knot breathing is qualitatively similar to the behavior we previously observed for knotted polymers in Couette flow [41]. We performed additional simulations of a polymer with $N = 256$ monomers and analyzed further configurational observables and their correlations to tumbling and knot breathing in Supplementary Section S2.

Figure 4c illustrates the process of tumbling (or recoiling) and how the knot size and relative x-position evolves over a typical recoiling process. The snapshots correspond to the trajectory shown in red in panel (b). When a chain is in a stretched state, then the monomer positions near the ends of the chains fluctuate more than central monomers due to the elongational forces. Knots tend to be tightened in such configurations, as the shear at the knot center position is likely to be large enough to tighten the knot. As the chain starts to recoil, the knot's relative x-position can reach an extreme value $x_{\mathrm{rel}} = 0$ or $x_{\mathrm{rel}} = 100\,\%$, where the local elongational forces weaken such that the knot center position is no longer stationary and the knot sizes increase. Note that the change in knot center position is small compared to the change in x_{rel} over time, indicating that the change in x_{rel} is dominated by the recoiling, not by the diffusion of the knot along the chain. As the recoiling process continues, the knot center position eventually reaches the opposite extreme x_{rel} position before the chain stretches again, likely leaving the knot in a more central relative x-position, thus fixing and tightening the knot again.

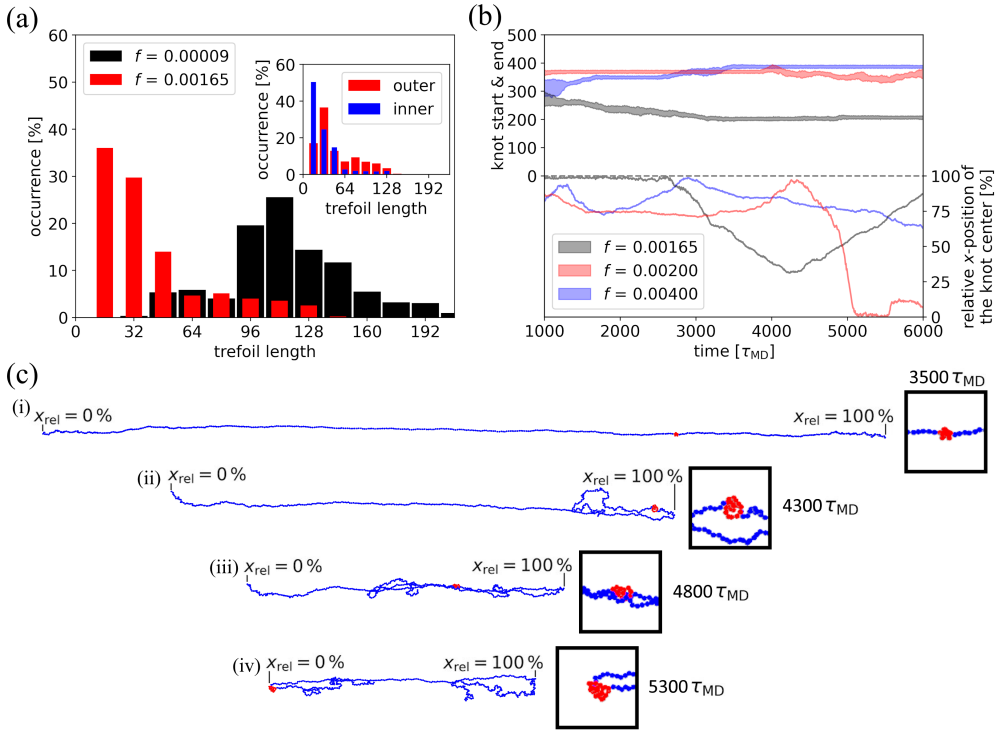


Figure 4. Tumbling effects in Poiseuille flow for $N = 512$: (**a**) Trefoil length distribution for two different forces f after the initial dynamic tightening. Knots decrease in size for stronger f, but still exhibit a long tail. The inset shows the trefoil length distribution for $f = 0.00165$ in more detail, where the distribution of knots with 'outer' and 'inner' relative x-positions are separated. The inner knots are tightened significantly stronger than outer knots. (**b**) Kymographs of the knot start and end positions and the knot center x_{rel} along the chain for three individual runs. Knot sizes fluctuate and grow whenever the knot center reaches the most extreme x-positions ($x_{rel} \approx 100\%$ or $x_{rel} \approx 0\%$). (**c**) Snapshots of the selected $f = 0.002$ simulation run shown in (**b**) during the tumbling process, with the knotted regions highlighted in red along with 3× zooms in the black boxes.

3.3. Effect of the Channel Width on Knot Tightening

Given the established result that Poiseuille flow generally leads to knot tightening, an important aspect of this process concerns the influence of channel width $2H$ on the tightening rate $\dot{K}_n(t)$. According to Equation (3), the maximal velocity is $v_x^{max}(z = 0) \propto fL_z^2$, so one would trivially expect $\dot{K}_n(t)$ to rise rapidly with increasing channel width L_z at fixed f. Less obvious is the influence of channel width on the tightening rate $\dot{K}_n(t)$ in channels with different width at *equal* mean shear rate $\bar{\dot{\gamma}}$.

In Figure 5, we show three different aspects characterizing the impact of channel width L_z on polymer chains in a Poiseuille flow that unambiguously demonstrate the increase in efficiency of knot tightening with growing channel width even in the case of equal mean shear rate $\bar{\dot{\gamma}}$. The efficiency of knot tightening, cf. Figure 5a, is found to increase steadily with the channel width increase as also does the degree of chain stretching (i.e., the effective shear-induced pulling on the knot), cf. Figure 5b, suggested by the growth of the two largest eigenvalues λ_1, λ_2 of the R_g^2-tensor. Since λ_1 describes the strongest stretching of the macromolecule along the flow, with growing λ_1, the chain segments of the macromolecule experience increasing difference in local flow velocity; therefore, any increase in λ_1 leads to a stronger shear-induced pulling force on the knot and and thus to increased tightening. The typical correlation time τ_0 of the end-to-end vector, $\vec{R}_e$, becomes also progressively shorter with growing channel width L_z at equal $\bar{\dot{\gamma}}$, see Figure 5c, indicating a faster renewal of the driven chain conformation with growing L_z. In Figure 5d, we compare the velocity profiles of the MPCD fluid particles in the narrow, $H/R_{g0} = 0.53$, and medium-wide

channel, $H/R_{g0} = 0.85$, demonstrating nearly perfect parabolic profiles of the flow. For medium-wide $H/R_{g0} = 0.85$, $f = 0.00103125$ corresponds to a mean shear $\bar{\dot{\gamma}}$ equal to that for $f = 0.00165$ in the narrow $H/R_{g0} = 0.53$ channel, while $f = 0.00165$ shows the effect of equal body force f for the two different half-widths H.

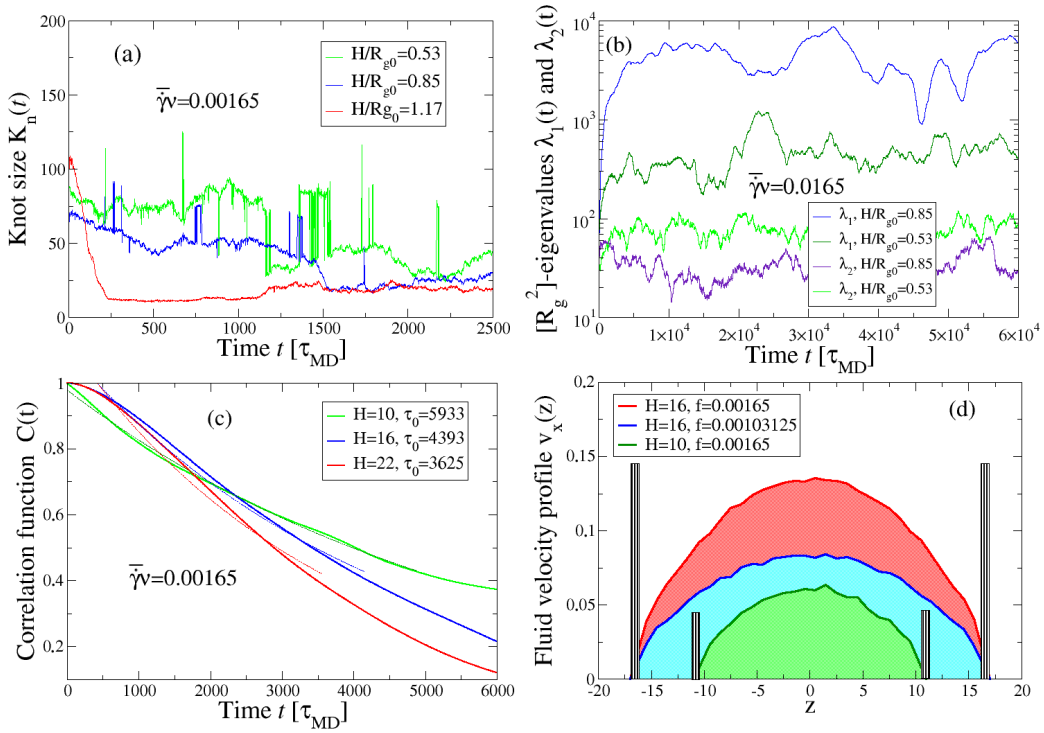


Figure 5. (**a**) Effect of channel width on knot tightening for three widths at equal mean shear rate $\bar{\dot{\gamma}} = 0.0165\nu^{-1}$. (**b**) The same for the degree of chain stretching, λ_1 and λ_2. Here $N = 512$. (**c**) The correlation function of the chains' end-to-end vector over time for three channel half-widths H. (**d**) Fluid velocity profiles $v_x(z)$ for channels with half-width ratio $H/R_{g0} = 0.53$ and $H/R_{g0} = 0.85$ at *equal body force* $f = 0.00165$ (green and red), as well as at *equal mean shear rate* $\bar{\dot{\gamma}}$ (green and blue) for $H/R_{g0} = 1.17$ and $H/R_{g0} = 0.85$.

Based on the established velocity profiles of Poiseuille flow, one may estimate the effective shear acting on the polymer at equal mean shear $\bar{\dot{\gamma}}$ by taking into account the distribution of chain segments exposed to local shear $\dot{\gamma}(z)$ (or $\dot{\gamma}(z/H)$) across the channel averaged over particular time intervals $\bar{P}_{mon}(z/H)$, Figure 6. We obtain the effective shear rate acting on the monomers by calculating the expectation value of the shear rate $|\dot{\gamma}(z/H)|$ with respect to the monomer distribution $\bar{P}_{mon}(z/H)$ across the channel averaged over a specific time interval of the simulation $\dot{\gamma}_{mon} = \int_{-1}^{1} \bar{P}_{mon}(z/H)|\dot{\gamma}(z/H)|d(z/H)$. As indicated by the insets to Figure 6a, the effective shear acting on the respective chain segments during the first 10 % of the simulation significantly increases with growing channel width H/R_{g0} notwithstanding the equal mean shear rate $\bar{\dot{\gamma}}$. The chains prefer to move towards the channel walls during the beginning of the simulations as can be seen by the more asymmetric monomer distribution $\bar{P}_{mon}(z/H)$ in panel (a). This leads to stronger shear experienced by the monomers $\dot{\gamma}_{mon}$ in wider channels since they can reach higher shear regions closer to the wall in units of z/H more easily. At later times, the Poiseuille flow progressively drives the chain towards $z = 0$, Figure 6b, in line with previous observations [55].

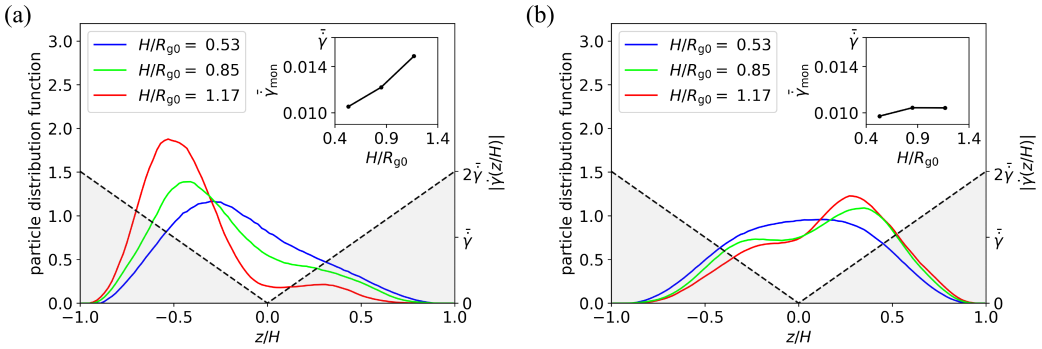


Figure 6. (**a**) Averaged distribution of chain segments during the first 10 % of the simulation run at equal mean shear rate $\bar{\dot{\gamma}}$ for 3 channel widths as indicated. The inset shows the cumulative shear acting on the monomers. (**b**) The same for the last 50 % of the run.

4. Methods for Experimental Verification

While there are many theoretical studies on knot topology and behavior in conjunction with DNA and proteins, there are currently very few experimental studies. Estimating the tightness of a knot in a polymer experimentally is challenging but feasible using techniques that probe conformational constraints, local density, and spatial distribution of the knot within the chain. Thus, there are several techniques to estimate the knot's spatial extent and how confined it is in the polymer backbone:

Atomic Force Microscopy (AFM) or *Cryo-Electron Microscopy (cryo-EM)* whereby polymers (like DNA or proteins) are deposited on a surface and imaged with tight knots appearing as *high-density regions* with distinct crossings. Spatial resolution then allows visual estimation of knot diameter or area [30].

Optical or Magnetic Tweezers where a single polymer chain is stretched by its ends. When a knot is pulled, it slides and tightens while resistance to sliding indicates entropic tightening. Measured force–extension curves of tighter knots result in force plateaus or sharp increases. Also the distance the knot migrates before getting trapped at an endpoint is indicative [64].

Fluorescence Resonance Energy Transfer (FRET). Attaching donor and acceptor dyes near suspected knot sites leads to higher FRET efficiency, e.g., with shorter distances (i.e., tighter knots) [65].

Nanopore Translocation, when knotted polymers are electrophoretically driven through nanopores. Tight knots slow down translocation and may cause blockade spikes in ionic current. The depth and duration of current blockade is linked to knot compactness [8].

Gel Electrophoresis (for DNA) shows that knotted DNA migrates slower than unknotted DNA, while tighter knots have reduced electrophoretic mobility. Combined with enzyme treatment (e.g., topoisomerases), this method can infer knot position and size [66].

A possible verification of the present computational results by the aforementioned methods would extend and corroborate our observations.

5. Conclusions

Given the insufficient understanding at present regarding the behavior and functionality of knots in macromolecules and proteins, and the influence of external forces on knot properties, the main objective of the present study is the clarification of the impact of pressure-driven Poiseuille flow on existing knots in linear polymer chains. To this end we carried out extensive mesoscale molecular dynamics simulations taking into account the hydrodynamic interactions by means of the Multi-Particle Collision Dynamics (MPCD) method. As a main result of the studies performed for a variety of body forces f, channel widths, L_z, and chain lengths N, one should point out the revealed general trend to *knot*

tightening which takes place beyond a certain critical body force f^{cr} and intensifies with growing f.

In addition, we have found that thermal fluctuations play a dramatic role in the dynamics of confined polymer chains under flow, for example, leading to tumbling motion associated with large conformational changes. The observed strong cross-correlation between intermittent chain tumbling and ensuing knot size fluctuations has been demonstrated to depend essentially on the knot position relative to the chain, indicating diminishing knot size stability as the proximity of the knot to the most extreme relative x-positions (largest x-position of all monomers or smallest x-position of all monomers) increases.

An interesting and non-trivial effect of the interplay between confinement and hydrodynamic interactions is also the observed impact of the channel width on the knot tightening rate $\dot{K}_n$. For polymers in the crossover from weak to strong confinement, H/R_{g0}, the efficiency of knot tightening is found to diminish with increasing confinement even at *equal* mean shear rate $\bar{\dot{\gamma}}$. Using the probability distribution of chain segments across the channel in conjunction with the local shear rate of the flow acting on them, we have shown that this result is a consequence of the steadily increasing shear acting on the chain conformation during tightening as the channel width grows [8,30,64–66].

Supplementary Materials: The following supporting information can be downloaded at: https://www.mdpi.com/article/10.3390/foundations5030028/s1, Supplementary Information; Video S1: A polymer consisting of 512 beads extending into a U-shaped conformation under Poiseuille flow. Body force $f = 0.0005$.

Author Contributions: Conceptualization, A.M.; methodology, A.M. and M.P.S.; software, A.M. and M.P.S.; validation, A.M. and M.P.S.; formal analysis, A.M. and M.P.S.; investigation, A.M. and M.P.S.; resources, A.M. and M.P.S.; data curation, A.M.; writing—original draft preparation, A.M. and M.P.S.; writing—review and editing, A.M. and M.P.S.; visualization, A.M. and M.P.S.; supervision, A.M.; project administration, A.M.; funding acquisition, A.M. All authors have read and agreed to the published version of the manuscript.

Funding: This research was funded by the Deutsche Forschungsgemeinschaft (DFG), SFB TRR 146 project number #233630050 and grant number VI 237/6–2.

Data Availability Statement: The data presented in this study are available on request from the corresponding author. The data are not publicly available due to exceedingly large file sizes of our trajectories.

Acknowledgments: Maurice Pierre Schmitt is grateful to the Deutsche Forschungsgemeinschaft (DFG) for funding (SFB TRR 146, project number #233630050). Andrey Milchev would also like to acknowledge partial support by the Deutsche Forschungsgemeinschaft (DFG) grant number VI 237/6–2. The authors gratefully acknowledge the computing time granted on the supercomputer MOGON II and III at Johannes Gutenberg University Mainz as part of NHR South-West. The authors acknowledge the use of ChatGPT (GPT-4o and GPT-4o mini) to enhance the language clarity and readability of the introduction and methods sections of this manuscript.

Conflicts of Interest: The authors have no conflicts of interest to disclose.

References

1. Faísca, P.F. Knotted proteins: A tangled tale of Structural Biology. *Comput. Struct. Biotechnol. J.* **2015**, *13*, 459–468. [CrossRef]
2. Micheletti, C.; Marenduzzo, D.; Orlandini, E. Polymers with spatial or topological constraints: Theoretical and computational results. *Phys. Rep.* **2011**, *504*, 1–73. [CrossRef]
3. Tubiana, L.; Alexander, G.P.; Barbensi, A.; Buck, D.; Cartwright, J.H.; Chwastyk, M.; Cieplak, M.; Coluzza, I.; Čopar, S.; Craik, D.J.; et al. Topology in soft and biological matter. *Phys. Rep.* **2024**, *1075*, 1–137. [CrossRef]
4. Arsuaga, J.; Vazquez, M.; Trigueros, S.; Sumners, D.W.; Roca, J. Knotting probability of DNA molecules confined in restricted volumes: DNA knotting in phage capsids. *Proc. Natl. Acad. Sci. USA* **2002**, *99*, 5373–5377. [CrossRef] [PubMed]

5. Arsuaga, J.; Vazquez, M.; McGuirk, P.; Trigueros, S.; Sumners, D.W.; Roca, J. DNA knots reveal a chiral organization of DNA in phage capsids. *Proc. Natl. Acad. Sci. USA* **2005**, *102*, 9165–9169. [CrossRef]
6. Marenduzzo, D.; Orlandini, E.; Stasiak, A.; Sumners, D.W.; Tubiana, L.; Micheletti, C. DNA–DNA interactions in bacteriophage capsids are responsible for the observed DNA knotting. *Proc. Natl. Acad. Sci. USA* **2009**, *106*, 22269–22274. [CrossRef]
7. Plesa, C.; Verschueren, D.; Pud, S.; van der Torre, J.; Ruitenberg, J.W.; Witteveen, M.J.; Jonsson, M.P.; Grosberg, A.Y.; Rabin, Y.; Dekker, C. Direct observation of DNA knots using a solid-state nanopore. *Nat. Nanotechnol.* **2016**, *11*, 1093–1097. [CrossRef]
8. Kumar Sharma, R.; Agrawal, I.; Dai, L.; Doyle, P.S.; Garaj, S. Complex DNA knots detected with a nanopore sensor. *Nat. Commun.* **2019**, *10*, 4473. [CrossRef]
9. Taylor, W.R. A deeply knotted protein structure and how it might fold. *Nature* **2000**, *406*, 916–919. [CrossRef]
10. Virnau, P.; Mirny, L.A.; Kardar, M. Intricate Knots in Proteins: Function and Evolution. *PLoS Comput. Biol.* **2006**, *2*, e122. [CrossRef]
11. Potestio, R.; Micheletti, C.; Orland, H. Knotted vs. Unknotted Proteins: Evidence of Knot-Promoting Loops. *PLoS Comput. Biol.* **2010**, *6*, e1000864. [CrossRef] [PubMed]
12. Mallam, A.L.; Rogers, J.M.; Jackson, S.E. Experimental detection of knotted conformations in denatured proteins. *Proc. Natl. Acad. Sci. USA* **2010**, *107*, 8189–8194. [CrossRef]
13. Boelinger, D.; Sulkowska, J.; Hsu, H.-P.; Mirny, L.; Kardar, M.; Onuchic, J.; Virnau, P. A Stevedore's Protein Knot. *PLoS Comput. Biol.* **2010**, *6*, e1000731. [CrossRef]
14. Virnau, P.; Mallam, A.; Jackson, S. Structures and folding pathways of topologically knotted proteins. *J. Phys. Cond. Matter* **2011**, *23*, 033101. [CrossRef]
15. Jarmolinska, A.I.; Perlinska, A.P.; Runkel, R.; Trefz, B.; Ginn, H.M.; Virnau, P.; Sulkowska, J.I. Proteins' Knotty Problems. *J. Mol. Biol.* **2019**, *431*, 244–257. [CrossRef]
16. Brems, M.A.; Runkel, R.; Yeates, T.O.; Virnau, P. AlphaFold predicts the most complex protein knot and composite protein knots. *Protein Sci.* **2022**, *31*, e4380. [CrossRef]
17. Frisch, H.L.; Wasserman, E. Chemical Topology 1. *J. Am. Chem. Soc.* **1961**, *83*, 3789–3795. [CrossRef]
18. Delbrück, M. *Knotting Problems in Biology*; Bellman, R.E., Ed.; American Mathematical Society: Providence, RI, USA, 1962; Volume 14, p. 55.
19. Vologodskii, A.V.; Lukashin, A.V.; Frank-Kamenetskii, M.D. Topological interaction between polymer chains. *Sov. Phys.-JETP* **1974**, *40*, 932–936.
20. Sumners, D.W.; Whittington, S.G. Knots in self-avoiding walks. *J. Phys. A Math. Gen.* **1988**, *21*, 1689. [CrossRef]
21. Mansfield, M.L. Knots in Hamilton cycles. *Macromolecules* **1994**, *27*, 5924–5926. [CrossRef]
22. Virnau, P.; Kantor, Y.; Kardar, M. Knots in globule and coil phases of a model polyethylene. *J. Am. Chem. Soc.* **2005**, *127*, 15102–15106. [CrossRef]
23. Adams, C.C. *The Knot Book*; American Mathematical Soc.: Providence, RI, USA, 1994.
24. Virnau, P. Detection and visualization of physical knots in macromolecules. *Phys. Procedia* **2010**, *6*, 117–125. [CrossRef]
25. Tubiana, L.; Orlandini, E.; Micheletti, C. Probing the Entanglement and Locating Knots in Ring Polymers: A Comparative Study of Different Arc Closure Schemes. *Prog. Theor. Phys. Suppl.* **2011**, *191*, 192–204. [CrossRef]
26. Foteinopoulou, K.; Karayiannis, N.C.; Laso, M.; Kroeger, M.; Mansfield, M.L. Universal Scaling, Entanglements, and Knots of Model Chain Molecules. *Phys. Rev. Lett.* **2008**, *101*, 265702. [CrossRef] [PubMed]
27. Meyer, H.; Horwath, E.; Virnau, P. Mapping onto Ideal Chains Overestimates Self-Entanglements in Polymer Melts. *ACS Macro Lett.* **2018**, *7*, 757–761. [CrossRef] [PubMed]
28. Zhang, J.; Meyer, H.; Virnau, P.; Daoulas, K.C. Can Soft Models Describe Polymer Knots? *Macromolecules* **2020**, *53*, 10475–10486. [CrossRef] [PubMed]
29. Coronel, L.; Orlandini, E.; Micheletti, C. Non-monotonic knotting probability and knot length of semiflexible rings: The competing roles of entropy and bending energy. *Soft Matter* **2017**, *13*, 4260–4267. [CrossRef]
30. Bornschlögl, T.; Anstrom, D.M.; Mey, E.; Dzubiella, J.; Forest, K.T. Tightening the Knot in Phytochrome by Single-Molecule Atomic Force Microscopy. *Biophys. J.* **2009**, *96*, 1508–1514. [CrossRef]
31. Ohta, S.; Alam, M.T.; Arakawa, H.; Ikai, A. Origin of mechanical strength of bovine carbonic anhydrase studied by molecular dynamics simulation. *Biophys. J.* **2004**, *87*, 4007. [CrossRef]
32. Sułkowska, J.I.; Sułkowski, P.; Szymczak, P.; Cieplak, M. Untying Knots in Proteins. *J. Am. Chem. Soc.* **2010**, *132*, 13954–13956. [CrossRef]
33. Liebetreu, M.; Ripoll, M.; Likos, C.N. Trefoil Knot Hydrodynamic Delocalization on Sheared Ring Polymers. *ACS Macro Lett.* **2018**, *7*, 447–452. [CrossRef]
34. Kuei, S.; Słowicka, A.M.; Ekiel-Jezewska, M.L.; Weinryb, E.; Stone, H.A. Dynamics and topology of a flexible chain: Knots in steady shear flow. *New J. Phys.* **2015**, *17*, 053009. [CrossRef]

35. Renner, C.B.; Doyle, P.S. Untying Knotted DNA with Elongational Flows. *ACS Macro Lett.* **2014**, *3*, 963–967. [CrossRef]
36. Di Stefano, M.; Tubiana, L.; Di Ventra, M.; Micheletti, C. Driving knots on DNA with AC/DC electric fields: Topological friction and memory effects. *Soft Matter* **2014**, *10*, 6491–6498. [CrossRef]
37. Narsimhan, V.; Klotz, A.R.; Doyle, P.S. Steady-state and Transient Behavior of Knotted Chains in Extensional Fileds. *ACS Macro Lett.* **2017**, *6*, 1285–1289. [CrossRef]
38. Klotz, A.R.; Soh, B.W.; Doyle, P.S. Motion of knots in DNA stretched by elongational fields. *Phys. Rev. Lett.* **2018**, *120*, 188003. [CrossRef]
39. Klotz, A.R.; Soh, B.W.; Doyle, P.S. An experimental investigation of attraction between knots in a stretched DNA molecule. *Europhys. Lett.* **2020**, *129*, 68001. [CrossRef]
40. Soh, B.W.; Klotz, A.R.; Doyle, P.S. Untying of Complex Knots on Stretched Polymers in Elongational Fields. *Mscromolecules* **2018**, *51*, 9562–9571. [CrossRef]
41. Milchev, A.; Schmitt, M.P.; Virnau, P. Effect of simple shear on knotted polymer coils and globules. *J. Chem. Phys.* **2024**, *161*, 224905. [CrossRef] [PubMed]
42. Tan, S. Monte-Carlo simulation of polymers in shear flow. *Polymer* **1999**, *40*, 695–700. [CrossRef]
43. Smith, D.E.; Babcock, H.P.; Chu, S. Single Polymer Dynamics in Steady Shear Flow. *Science* **1999**, *283*, 1724–1727. [CrossRef] [PubMed]
44. Lyulin, A.V.; Adolf, D.B.; Davies, G.R. Brownian dynamics simulations of linear polymers under shear flow. *J. Chem. Phys.* **1999**, *111*, 758. [CrossRef]
45. Kong, X.; Han, Y.; Chen, W.; Cui, F.; Li, Y. Understanding conformational and dynamical evolution of semiflexible polymers in shear flow. *Soft Matter* **2019**, *15*, 6353–6361. [CrossRef]
46. Jeong, S.H.; Cho, S.; Baig, C. Chain rotational dynamics in dilute polymer solutions and melts under shear flow. *Polymer* **2023**, *281*, 126101. [CrossRef]
47. Srivastva, D.; Nikoubashman, A. Flow Behavior of Chain and Star Polymers and Their Mixtures. *Polymers* **2018**, *10*, 599. [CrossRef]
48. Cannavacciolo, L.; Winkler, R.G.; Gompper, G. Mesoscale simulations of polymer dynamics in microchannel flows. *Europhys. Lett.* **2008**, *83*, 34007. [CrossRef]
49. Grest, G.S.; Kremer, K. Molecular dynamics simulation for polymers in the presence of a heat bath. *Phys. Rev. A* **1986**, *33*, 3628(R). [CrossRef] [PubMed]
50. Malevanets, A.; Kapral, R. Mesoscopic model for solvent dynamics. *J. Phys. Chem.* **1999**, *110*, 8605–8613. [CrossRef]
51. Gompper, G.; Ihle, T.; Knoll, D.M.; Winkler, R.G. Multi-particle collision dynamics: A parrticle-based mesoscale simulation approach to the hydrodynamics of comlex fluids. *Adv. Polym.* **2009**, *221*, 1–87.
52. Andersen, L.; Lorenz, C.; Travesset, J. General purpose molecular dynamics simulations fully implemented on graphics processing units. *J. Comput. Phys.* **2008**, *227*, 5342–5359. [CrossRef]
53. Padding, J.T.; Louis, A.A. Hydrodynamic interactions and Brownian forces in colloidal suspensions: Coarse-grained over time and length svvales. *Phys. Rev. E* **2006**, *74*, 031402. [CrossRef]
54. Ihle, T.; Knoll, D.M. Stochastic rotational dynamics: A Galilean-invariant mesoscopic model for fluid flow. *Phys. Rev. E* **2001**, *63*, 020201. [CrossRef]
55. Jendrejack, R.M.; Dimalanta, E.T.; Schwartz, D.C.; Graham, M.D.; de Pablo, J.J. DNA Dynamics in a Microchannel. *Phys. Rev. Lett.* **2003**, *91*, 038102. [CrossRef]
56. Ranguelov, B.; Petkov, P.; Milchev, A. Flow-Induced Vesicle Translocation through a Narrow Slit–Transit Time Scaling Relations. *Langmuir* **2025**, *41*, 15849–15856. [CrossRef] [PubMed]
57. Tubiana, L.; Polles, G.; Orlandini, E.; Micheletti, C. Kymoknot: A web server and software package to identify and locate knots in trajectories of linear or circular polymers. *Eur. Phys. J. E* **2018**, *41*, 72. [CrossRef]
58. Klotz, A.R.; Estabrooks, B. Revisiting the second Vassiliev (In) variant for polymer knots. *J. Phys. A Math. Theor.* **2024**, *57*, 245002. [CrossRef]
59. Herschberg, T.; Pifer, K.; Panagiotou, E. A computational package for measuring Topological Entanglement in Polymers, Proteins and Periodic systems (TEPPP). *Comp. Phys. Commun.* **2023**, *286*, 108639. [CrossRef]
60. Meluzzi, D.; Smith, D.E.; Arya, G. Biophysics of knotting. *Annu. Rev. Biophys.* **2010**, *39*, 349–366. [CrossRef]
61. Humphrey, W.; Dalke, A.; Schulten, K. VMD: Visual molecular dynamics. *J. Mol. Graph.* **1996**, *14*, 33–38. [CrossRef]
62. Winkler, R.G. Semiflexible Polymers in Shear Flow. *Phys. Rev. Lett.* **2006**, *97*, 128301. [CrossRef]
63. Dai, L.; Doyle, P.S. Trapping a Knot into Tight Conformations by Intra-Chain Repulsions. *Polymers* **2017**, *9*, 57. [CrossRef] [PubMed]
64. Wang, H.; Li, H. Mechanically tightening, untying and retying a protein trefoil knot by single-molecule force spectroscopy. *Chem. Sci.* **2020**, *11*, 12512–12521. [CrossRef] [PubMed]

65. Bikerdal, V. Folding and unfolding of G-rich DNA knots using single molecule. *Biophys. J.* **2024**, *123*, 4a. [CrossRef]
66. Cebrián, J.; Kadomatsu-Hermosa, M.J.; Castán, A.; Martínez, V.; Parra, C.; Fernández-Nestosa, M.J.; Schaerer, C.; Martínez-Robles, M.-L.; Hernández, P.; Krimer, D.B.; et al. Electrophoretic mobility of supercoiled, catenated and knotted DNA molecules. *Nucleic Acids Res.* **2014**, *43*, e24.

Disclaimer/Publisher's Note: The statements, opinions and data contained in all publications are solely those of the individual author(s) and contributor(s) and not of MDPI and/or the editor(s). MDPI and/or the editor(s) disclaim responsibility for any injury to people or property resulting from any ideas, methods, instructions or products referred to in the content.